revised manuscript. Layout mimicks the paper to be published. N.S. 2004 04 27

Macromol. Chem. Phys. **2004** , *205(?)*, ???-???

Full Paper: Highly oriented high-pressure injection-molded (HPIM) rods from polyethylene (PE) are heated until the discrete small-angle X-ray scattering (SAXS) has vanished. Thereafter non-isothermal and isothermal crystallization is investigated *in situ* by means of ultra small-angle X-ray scattering (USAXS). Orientation of the crystallites can be controlled by choice of the melt annealing temperature (shish-kebab model: memory, or self-nucleation effect caused by stable shishs). Both the scattering patterns and the multidimensional chord distribution function (CDF) are interpreted. A three-stage model of crystallization is developed. This model comprises row structure nucleation, almost statistical insertion of extended lamellae, and finally the insertion of blocky crystallites.

It is found that the nanostructure evolution in the isotropic fraction of the material is the same as in the highly oriented one. The lateral extension of the lamellae is largest during isothermal crystallization. Correlation among domains is increased by non-isothermal crystallization. The shishs in the core of the HPIM rod appear less stable than those in the shell. Lobe-shaped reflections observed during and after quenching are not due to an orientation distribution of layer stacks, but reflect a correlation between long period and lateral extension of crystallites. During quenching a lateral modulation of the layer peaks in the CDF grows strong and shows the arrangement of block-shaped crystals proposed by Strobl to be the precursors of lamellae. The thin crystals formed during rapid cooling are built from a central block surrounded by one or two rings of satellites. The long period observed in the scattering pattern during quenching is caused from correlations among crystalline blocks in a chain, and not from correlations among lamellae.

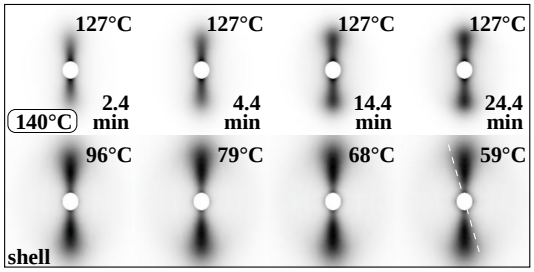

USAXS scattering patterns from the isothermal, oriented crystallization of HPIM–PE material (bottom row: during final quenching after 30 min at 127°C). This sample from the shell of the rod was melt-annealed at T_{max} =140°C. Each pattern shows the range $|s_{12}|, |s_3| \leq 0.04\ \mathrm{nm}^{-1}$. The fiber axis, s_3, is vertical.

Oriented quiescent crystallization of polyethylene studied by USAXS. Part 1: Observations of nanostructure evolution

Norbert Stribeck[*1], *Armando Almendarez Camarillo*[1], *Sabine Cunis*[2], *Rüdiger K. Bayer*[3], *Rainer Gehrke*[4]

[1] Institut für Technische und Makromolekulare Chemie, Universität Hamburg, Bundesstr. 45, 20146 Hamburg, Germany, Fax: +49 40-4123-6008, eMail: Norbert.Stribeck@desy.de
[2] Max–Planck Institut für Kolloide und Grenzflächen, c/o HASYLAB, 22603 Hamburg, Germany
[3] Institut für Werkstofftechnik, Universität GH Kassel, 34109 Kassel, Germany
[4] HASYLAB at DESY, Notkestr. 85, 22603 Hamburg, Germany

Keywords: crystallization; disorder; orientation; nanostructure evolution; SAXS

Introduction

The crystallization of polymers, and of polyethylene in particular, has been studied for almost 50 years. However, many questions remained unanswered, because for a long time the available methods provided insufficient data. Of particular interest in the case of crystallization is the evolution of the nanostructured morphology. Synchrotron radiation as a powerful X-ray source has promised[1] to elucidate this evolution, and since the year 2000 stable sources and beam lines with qualified optics are widely used. Since then *in situ* studies of the crystallization of polymers are enjoying a renaissance.

Many of these investigations focus on the quiescent crystallization of isotropic materials. From principal reasons the data recorded in such experiments require early modeling for the interpretation of the results (e.g. the assumption of "ideal lamellar stacks"). Utilizing the experiment presented here, we expect to become able both to assess the validity of such models, and to determine several parameters of the nanostructure without presupposition.

Discussing oriented crystallization, we do not investigate the effect of transcrystallization that is characterized by induc-

tion of orientation due to foreign domains,[2–5] nor do we study the field of shear induced crystallization.[6–8] We start from highly oriented polyethylene (PE) rods. During the melting of such materials nanostructure evolution has been reported by Rueda et al.[9] and some of us.[10] After heating to 150°C we have found isotropic crystallization, whereas Rueda et al. have reported oriented crystallization after heating to 130°C.

Such "memory" or "self-nucleation effect" is well–known,[11–14] but is rarely employed for the X–ray investigation of anisotropic, quiescent crystallization. Nevertheless, the information content of the resulting scattering patterns is much higher than that from isotropic materials. Shape, size and correlation of the ensemble of crystalline domains become directly accessible in the patterns.

In this study we focus on the transition between oriented and isotropic crystallization as a function of the melting temperature, and we investigate the process of crystallization in intervals of minutes. Both the induction period and the relative variation of scattering power cannot be studied on the available instrument (HASYLAB Hamburg, beam line BW4). The induction period is inaccessible, because the signal-to-noise ratio of the scattering data recorded near the melting point is low. In 1985 already, Vonk[15] has pointed out that in this case oscillations of density as a function of space deduced from the scattering data may be artefacts. Thus, near the melting point, a very high brilliant source is required. Once crystallization has started, the scattering intensity is increasing very strongly, and the gas–filled detector becomes the limiting factor. In order not to overload it, the gas amplification must continuously be adjusted. Thus background correction turns into a rough estimate.

Somani et al.[6] investigate crystallization using a more advanced setup (NSLS BNL Brookhaven, beam line X27C, MAR-CCD detector). They induce oriented crystallization by shear–flow, and not by temperature change. Based on their data they develop a model in which nucleation sites are random in volume and impingement of lamellae stops the lateral growth. Wu et al.[16] study nanostructure evolution *in situ* during fiber spinning, project the scattering pattern on the meridian (cf.[17,18]), and analyze the correlation function.[19,20] Their results indicate that crystallization is coupled to defect creation and transport. With our experiments we are aiming at similar results in the field of the quiescent crystallization of polymers.

Experimental

Highly oriented polyethylene (PE) rods are prepared from commercial material, cautiously melt–annealed in a furnace, and finally crystallized in the synchrotron beam of an ultra small–angle X–ray scattering (USAXS) beam line. In the majority of the experiments the orientation is preserved, although the nanostructure changes completely. The nanostructure evolution of these materials during melting has been reported in earlier work.[10,21]

Commercial polyethylene was used for our experiments (Lupolen 6021 D, BASF, M_W=182000 g/mol, M_n=25000 g/mol, density 0.962 g/cm^3, melt index 0.2). In order to achieve high orientation, an equilibrated, low–temperature melt (160°C) is injected into a cold mold. The pressure–time diagram of the molding process is shown in Figure 1. Maximum mold pressure is 444 MPa and final mold pressure 336 MPa after 180 s. In the differential scanning calorimetry (DSC) the material exhibits bimodal melting with peak maxima at 131°C and 141°C.

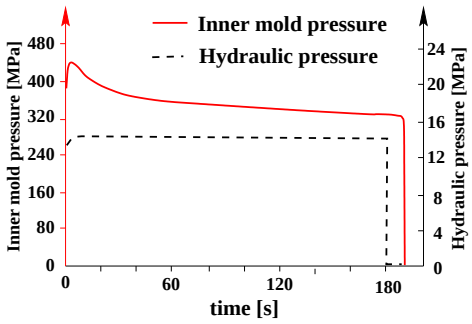

Figure 1: Pressure–time diagram of the injection molding process.

Rods of 10 cm length and a diameter of 6 mm are obtained. Inspection by the eye exhibits a core–shell structure with a core diameter of 2.5 mm. Samples for the USAXS investigation are sectioned from the shell and the core of the rod, respectively, using a low–speed diamond saw.[10]

USAXS is performed in the synchrotron beam line BW4 at HASYLAB, Hamburg, Germany. The wavelength of the X–ray beam is 0.1381 nm. USAXS images are collected by a two–dimensional position sensitive Gabriel detector (512×512 pixels of $0.4\times0.4\,\mathrm{mm}^2$) (from European Molecular Biological Laboratory, EMBL). The sample–to–detector distance is set to 13005 mm. The minimal accessible scattering angle corresponds to a d–spacing of 800 nm. The maximal scattering angle corresponds to 17 nm.

Samples of 2 mm thickness are wrapped in aluminum foil and subjected to a temperature program using a furnace equipped with two heating cartridges and air cooling that is provided at the beam line. The image accumulation period is 117 s. Data storage consumes 3 s.

Because of the low dynamic range of the detector, its gas amplification factor is continuously decreased during measurement in order to always record images with a sufficient signal–to–noise ratio, required for the intended nanodomain analysis. Due to this procedure, background subtraction is turned into a guess, but we trust in the ability of the spatial filtering algorithm developed by one of us[22,23] to compensate imbalances, as has been found in earlier work.[24] Obviously, on the basis of such data it is impossible to discuss changes of the scattering power.

Data evaluation

The two–dimensional scattering patterns are normalized to detector efficiency and incident beam flux. The mentioned variation of the detector bias during the experiment has no visible influence on the normalization to detector efficiency. Before the normalization both several detector wires and a less-sensitive area are clearly depicted in each of the images from the old Gabriel detector. After normalization all the patterns look smooth. An average machine background is recorded (averaged over the interval of detector gain variation). Sample absorption is estimated on the basis of the readings of ionization chambers before and after the sample, and a guessed machine background is subtracted by taking the estimated absorption factor and the average machine background for granted. This awkward procedure is the only way to carry out our studies at HASYLAB, as long as materials science of soft condensed matter does not receive the modern equipment that is a standard in other fields since several years.

Blind areas are masked in the images. Each image is centered and aligned. Four–quadrant averaging is carried out. The remnant central blind spot from the beam stop is filled. Data for extrapolation are supplied by radial basis function approximation.[25] In similar manner a smooth extrapolation is computed for wider scattering angles. The final scattering patterns covers the region $|s_{12}|$, $|s_3| < 0.09\,\mathrm{nm}^{-1}$ with the modulus of the scattering vector $\mathbf{s}$ defined by $s = \sqrt{s_{12}^2 + s_3^2} = (2/\lambda)\sin\theta$, and 2θ being the scattering angle. As described earlier[22] the scattering intensity is projected onto the (s_1, s_3)–plane, multiplied by s^2, then regridded to 512 x 512 pixels. The two–dimensional (2D) density fluctuation background is determined (Butterworth low pass filter of 1st order with a cut–off frequency $r_c = 1$ in units of pixels) and subtracted, resulting in an interference function $G(s_{12}, s_3)$. Background filtering is carried out in two iterated steps for each image. Two steps are required to balance the interference function, and thus to compensate for the inaccuracy concerning the subtraction of the machine background. By selecting not more than two steps we expected not to touch the diffuse scattering effect of uncorrelated crystalline domains, which otherwise might have become considered background. $G(s_{12}, s_3)$ is subjected to 2D Fourier transformation yielding the 3D chord distribution function (CDF), $z(r_{12}, r_3)$.

The discussion of the CDF in terms of the nanodomain topology[10, 22, 26, 27] within the sample is straightforward, since the CDF is defined[22] by the Laplacian of Vonk's multidimensional correlation function.[28] As such it presents the autocorrelation of the surfaces from the (nanosize) domains in space in a similar manner as Ruland's interface distribution function does[29–31] for one–dimensional structures as a function of distance. For samples with fiber symmetry, the CDF $z(r_{12}, r_3)$ is a function of two co-ordinates only (transverse direction r_{12}, and fiber direction r_3). Therefore it can be displayed by means of contours in a plane. Positive peaks found in the vicinity of the origin are size distributions of the primary domains. Thus their size, shape and orientation in space are depicted. Negative peaks following farther out exhibit "long periods", i.e. the distance of two adjacent domains from each other. Subsequent positive peaks describe the size and orientation of superdomains (i.e. assemblies made from two primitive domains separated by a rather probable distance and measured from the beginning of the first to the end of the second domain), and correlations among domains more distant are manifested in consecutive peaks at longer distance. As has been expatiated in several papers,[10, 22, 27] the CDF is computed from the scattering intensity $I(\mathbf{s})$ by

$$z(r_1, r_3) = -\mathscr{F}^2\left(4\pi^2\left(s_1^2 + s_3^2\right)\{I(\mathbf{s})\}_2(s_1, s_3) - B(s_1, s_3)\right), \quad (1)$$

with the projection of the scattering intensity on the representative (s_1, s_3)–plane,

$$\{I(\mathbf{s})\}_2(s_1, s_3) = \int I(\mathbf{s})\, ds_2, \quad (2)$$

the factor $-4\pi^2\left(s_1^2 + s_3^2\right)$ being equivalent to the Laplacian in physical space, $B(s_1, s_3)$ describing a background determined by spatial frequency filtering of the function $4\pi^2\left(s_1^2 + s_3^2\right)\{I(\mathbf{s})\}_2(s_1, s_3)$, and $\mathscr{F}^2(\,)$ denoting a 2D Fourier transformation.

Results and Discussion

Scattering Patterns

Non–isothermal crystallization experiments

Figure 2 shows a selection of scattering patterns taken during the non-isothermal crystallization experiments.

Melting. The top row in Figure 2 demonstrates the known melting process[9, 10] of HPIM PE materials. We observe the typical high long period of 100 nm vanishing. No discrete scattering is observed, when the selected melt annealing temperature T_{max} (here: 140°C) is reached. After keeping the temperature constant for 2 min, the sample is subjected to cooling at a constant rate of 2°C/min. No change is observed before the temperature drops to 127°C.

Statistical crystallization of extended lamellae. Here we demonstrate strong indications for the shish–kebab model, non–uniform long periods but uniform extension of crystalline layers.

At 125°C (Figure 2, second row, first pattern) we observe the beginning crystallization. A perfect orientation of the lamellae is obvious. No reflection maximum, but an intensity ridge on the meridian is observed. Thus the long period distribution is clearly non–uniform, and the positions at which crystal lamellae are created are almost random. The observed oriented recrystallization is readily explained by the shish–kebab

model. During melt annealing at 140°C only lamellae (kebab) are melted, whereas the oriented backbones (shish) persist, and at lower temperature provide for the orientation of crystallites.

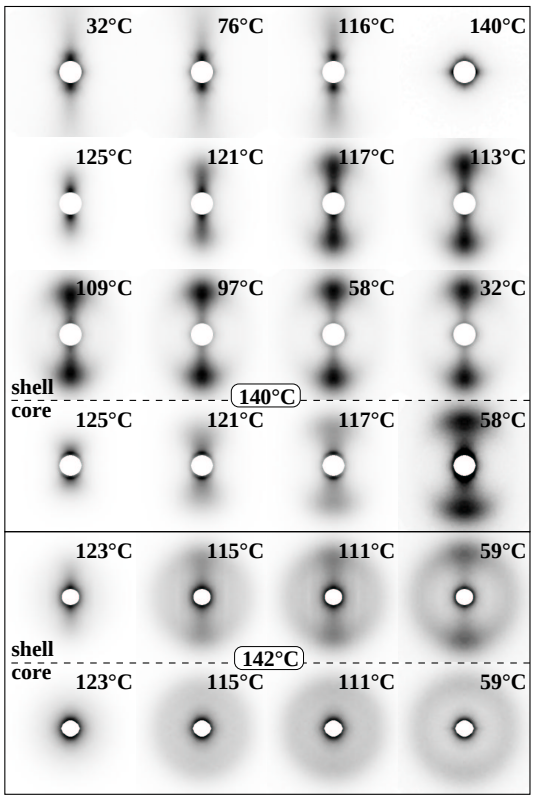

Figure 2: USAXS patterns taken during melting (top row) and subsequent non–isothermal crystallization of injection molded PE rods. Both samples from the core and the shell, respectively, are studied. Each pattern shows the region $|s_{12}|, |s_3| \leq 0.04$ nm^{-1}. The fiber axis, s_3, is vertical. The four top rows demonstrate the evolution during heating to T_{max} =140°C and subsequent crystallization. The two bottom rows show results from crystallization experiments after heating to T_{max} =142°C. Both heating and cooling rates are 2°C/min.

At 121°C the length of the intensity ridge has grown far beyond the extension of the discrete scattering found in the original HPIM–PE rod. Still, its "beam shape" indicates the continued non–uniform long period distribution, now with shorter long periods added. The lateral extension of the crystalline lamellae is still large.

Correlated crystallization of imperfect lamellae. At the ends of the intensity beam we, nevertheless, observe first indications of both a widening, and the creation of an intensity maximum. We conclude that the formation of less extended but more correlated crystallites has begun. On continued temperature decrease more and shorter long periods are added.

Finally, a nanostructure has formed that is completely different from the one of the original PE rod. Only the perfect orientation is preserved, and in this sense the process may be denoted a *re*–crystallization.

Similar process reported in the literature. Our time–resolved experiments on HPIM–PE thus result in a process description of the crystallization that is almost identical to the one given by Rueda et al.[9] after studying a different material in a different experiment. In their work Rueda et al. study isotropic low–pressure injection molded PE during melting and deduce both the two crystallite populations (extended layers and more granular ones), and a random nucleation of the extended lamellae. In their experiment the two populations are identified after the observation of two clearly separated peak maxima, the origin of which is reconstructed from their melting behavior. In our experiment we are able to identify them directly in the course of our time resolved crystallization experiment.

Discussing the stages of crystallization in PE with shish-kebab structure. Similar to what Rueda et al.[9] have reported, we have studied the melting behavior in earlier work[10] and drawn indirect conclusions concerning the crystallization. Our HPIM–PE has not shown two USAXS peaks, but only one long period on an intensity ridge. From the study of the peak during melting we could not deduce statistical nucleation. On the contrary, we have found periodical nucleation (a row structure) with a lattice constant of 90 nm. Nevertheless, after these primary sites were occupied, we have observed random nucleation that manifests itself in the intensity ridge.

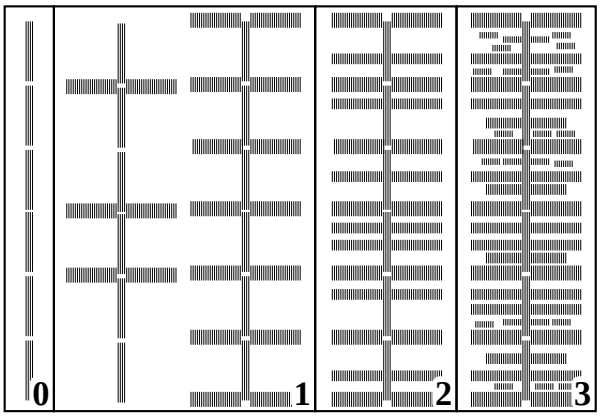

Figure 3: Steps of the oriented crystallization of PE with shish-kebab structure. A shish (0) with imprinted lattice structure promotes oriented crystallization. In the first step (1) thick and extended lamellae are formed on a lattice (row nucleation) with long repeat. After that (2) layers are generated at more or less random positions, but still show considerable extension. Finally (3) thin and grainy layers are formed at positions that are somewhat less randomly chosen.

The apparent conflict is resolved if we assume that during HPIM — in contrast to low pressure injection molding — the nanostructure is frozen in in an early stage. In this case the analysis of the melting behavior of a HPIM sample results in information on the history of the first layers formed. The further process can then either be studied by analysis of such injection molded materials used by Rueda et al.,[9] or, as is done in the present study, directly by analysis of data from a time resolved, oriented, and quiescent crystallization experiment.

Provided that the assumption on the earliest stage of crystallization being preserved in the HPIM material holds, our data are compatible with the following proposition for the process of non-isothermal, quiescent crystallization of PE with shish-kebab structure (cf. Figure 3)

1. Initial extended lamellae growing from the backbone on the lattice sites of a row structure.

2. Almost statistical nucleation of extended lamellae growing from the backbone.

3. Insertion of blocky crystallites in remnant amorphous zones.

After such a process the long period extracted from the scattering pattern will be dominated by the best correlated, most frequent clusters of crystalline domains, as is controlled by the materials processing.

Recrystallization. Similar nanostructure in core and shell material. In the fourth row of Figure 2 we present selected scattering patterns from a non–isothermal crystallization experiment of core material from the rod of HPIM–PE subjected to still the same temperature program. Although the scattering pattern of the initial core material only exhibits some oriented diffuse scattering close to the primary beam, the recrystallization shows the same features and step as the shell material. There are only two differences. Firstly, the extended width of the reflection generated in step 3 shows that the crystallites generated in the core are even smaller than the ones generated inside the shell material. Secondly, a fraction of the scattering from the original HPIM material has returned (cf. the central parts of the scattering patterns). In section we will demonstrate that the reconstruction of the HPIM structure is related to the presence of unmelted uncorrelated lamellae at 140°C, the diffuse particle scattering of which is unobtrusive in the scattering pattern.

Elevated melting temperature. The mechanism of isotropization. From our earlier work[10] we remember that after melt-annealing at 150°C the material is crystallizing isotropically. Now the question is, if the orientation distribution of the layers is going to widen as a function of increasing melt annealing temperature, or if there is a transition interval of temperature, in which both highly oriented and isotropic regions are present in the material. The fifth row of Figure 2 shows the result for the crystallizing shell material after fusing at 142.4 ± 0.5°C. We observe the creation of both the highly oriented and an isotropic nanostructure. Thus the process is not governed by orientation relaxation of backbones in a low viscosity melt. Instead, the shishs are melted and where they have vanished the material is crystallizing isotropically.

Similarity of oriented and unoriented nanostructures. It is worth to be noted, that during the course of the experiments the reflection ring of the isotropic component is crossing exactly where we find the point–like reflections of the oriented component. The movements of ring and two-point diagram are coupled. Thus the nanostructure evolution of the oriented crystallization appears to be conforming with that of the isotropic crystallization.

Elevated melting temperature. Shishs of core material are less stable. Also a sample from the core of the HPIM PE rod has been melt-annealed at 142.2 ± 0.5°C and subjected to non–isothermal crystallization. In contrast to the corresponding experiment with shell material, we here only observe isotropic crystallization. Because of the fact that both the mass of the core sample was bigger and the actual melt annealing temperature was not higher than with the shell sample, we assume that the backbones in the core material are less stable than those in the shell material. Thus, by application of heat from the outside, it might be possible to reduce the inhomogeneity of HPIM rods in an annealing step without loss of preferred orientation.

In two other experiments we have decreased the upper limit of the melt annealing temperature interval in which oriented crystallization is observed. All samples heated to 145°C show the isotropic crystallization behavior demonstrated in the bottom row of Figure 2.

Isothermal crystallization

We have heated a sample from the shell of the HPIM rod, kept it for 2 min at 140.6 ± 0.5°C, and quenched it to 127°C. After 40 s of cooling the extremum of the undershoot (120°C) is reached. After further 40 s the thermocouple shows the preset crystallization temperature. We estimate that a homogeneous temperature distribution inside the sample is reached 2 min after starting the cooling procedure. This assessment is based on the melting behavior of the sample: Whenever we approach a temperature level at which part of the sample is molten, a constant integral counting rate in the X–Ray detector is reached 90 s thereafter.

Observations. The central part of selected scattering patterns collected during the time resolved experiment are presented in Figure 4. The images in the top row show the nanostructure evolution during the isothermal phase of the experi-

ment. The time specified is related to the middle of the exposure interval. The first discrete USAXS is observed 2.4 min after the temperature jump. An intensity ridge is extending along the meridian of the scattering pattern up to rather high values of $|s_3|$. Thus the first pattern already indicates a wide, almost statistical distribution of long periods, similar to the one found in the non–isothermal experiments at 121°C (cf. Figure 2). Nevertheless, here the lateral extension of the layers is wider than those found in the non–isothermal crystallization experiments. During the first 10 min the scattering pattern does not change considerably. Starting from the pattern taken at 14.4 min we observe the "head" formation at both ends of the intensity beam, which is characteristic for the third step in quiescent crystallization. Nevertheless, here this feature is much weaker than that found during non-isothermal crystallization.

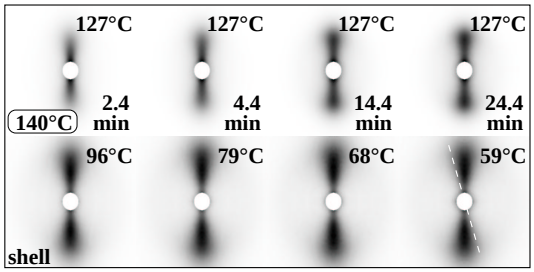

Figure 4: USAXS scattering patterns from the isothermal, oriented crystallization of HPIM–PE material (bottom row: during final quenching after 30 min at 127°C). This sample from the shell of the rod was melt-annealed at T_{max} =140°C. Each pattern shows the range $|s_{12}|, |s_3| \leq 0.04$ nm^{-1}. The fiber axis, s_3, is vertical.

After 30 min the isothermal phase has been interrupted, and the sample quenched to ambient temperature. A selection of the scattering patterns taken during this phase is demonstrated in the bottom row of Figure 4. Again, the scattering patterns show that during cooling the perfection of the newly added crystals is constantly decreasing.

The lobe shape of the reflections. Let us now discuss the lobe shape of the reflections observed during quenching of this sample. It appears worth to be noted that none of the images in the lower row of Figure 4 demonstrate an orientation distribution of long periods about the fiber axis. The *in situ* data show that the lobe shape is simply a result of a peculiar correlation of layer extension and long period. The lobe head is formed from the late, thin, and narrow crystallites. The lobe stem is related to the arrangement of thick and extended crystalline lamellae. As a result, the dashed line put into the last pattern is not related to an upper tilt angle of lamellae. Instead, from its inclination we estimate that the fourfold lattice constant of a layer cluster is close to the lateral extension of the lamellae contained in it.

Approaching quantitative analysis for heterogeneous nanostructures. Already an interpretation of the scattering patterns has demonstrated the considerable heterogeneity of the nanostructure with only few[32] neighboring crystallites correlated to each other in a cluster. Because of this severely distorted nanostructure it makes little sense to determine peak positions and widths from the few scattering patterns, for which these parameters may be extracted with some significance. Therefore we transform the anisotropic scattering patterns to the multidimensional chord distribution function that shows both the domains and their correlation in real space.[10, 22]

Interpretation of the CDF

Observations during melting

Incomplete erasure of lamellae. Close to the selected melt annealing temperature none of the samples shows discrete USAXS. Nevertheless, after computation of the CDF we find that in some cases a weakly correlated rest of lamellar nanostructure has still been preserved (comparable to Figure 5a).

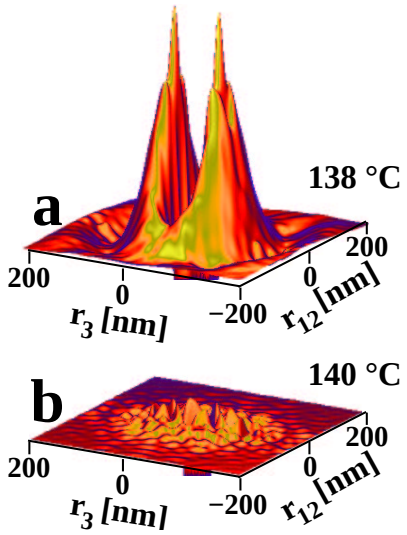

Figure 5: CDF during melting of HPIM PE shell material. At 138°C some weakly correlated lamellae are still present. At 140°C they are molten.

Only for such samples (e.g. the core material melt–annealed at 140°C and subjected to non–isothermal crystallization) we observe partial reconstruction of the HPIM nanostructure during crystallization. We suppose that the reason for imperfect erasure of the nanostructure is either a higher sample mass or an inferior heat contact between sample and furnace.

Remnant layer structure and lateral offset of HPIM lamellae. Figure 5 demonstrates typical CDFs collected close to the chosen melt annealing temperature during the melting

phase. Only close to the melting point (Figure 5a) the crystalline and the amorphous layers may be discriminated in the CDF. Centered on the meridian and closer to the origin we observe a triangular "layer peak" at $(r_{12}, r_3) = (0\,\text{nm}, \pm 40\,\text{nm})$. A little bit further out we find a split peak on both sides of the meridian at $(r_{12}, r_3) = (\pm 15\,\text{nm}, \pm 55\,\text{nm})$. The former peak describes the correlation between the "top" and the "bottom" surface of a crystalline layer. The latter one is related to amorphous layers. It is split, because there is a high probability to find the top and the bottom surfaces of amorphous layers shifted by 15 nm in the direction transverse to the fiber axis (cf. Figure 6b). Thus the best correlation is obtained after moving the top surface first down by 55 nm, then laterally by another 15 nm. The effect has already been observed in our earlier experiments,[10] but not been reported.

In the favorable case, after reaching the selected melt annealing temperature the remnant particle structure has vanished (Figure 5b).

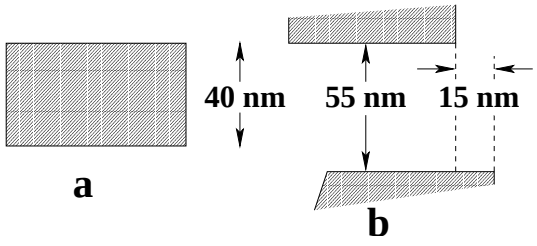

Figure 6: The latent layer structure just before the melting of the crystalline layers. The crystalline lamella (a) results in the central triangular peak of the CDF (cf. Figure 5a). The top and bottom surfaces of the amorphous layers (b) correlate best when shifted in lateral direction, additionally.

CDFs from the crystallization experiments

Principal observations. Figure 7 shows the CDF of the shell material during non–isothermal crystallization at a temperature of 117°C. Figure 7a views the CDF surface from the top. In this case the elevated peaks describe shape and arrangement of the nanodomains. The observed triangle-shaped peaks parallel to the equator are typical for layers extended in the direction perpendicular to the fiber axis. Loss of correlation among layers is indicated by loss of the peak heights as a function of increasing distance from the equator.

Two lamellae are correlated to each other on an average. This poor correlation is demonstrated very clearly in the logarithmic representation of peak height (Figure 7c). The long period peaks are observed after turning the CDF surface upside down (Figure 7b). Here as well the poor correlation is obvious.

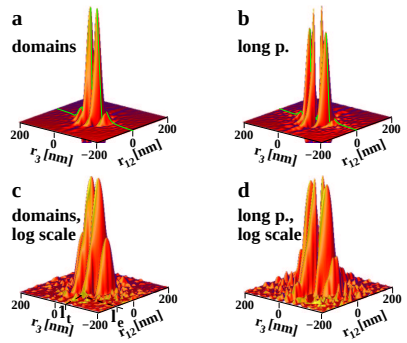

Figure 7: CDF at 117°C during non-isothermal crystallization of the shell material. (a) The domains are lamellae, but with short range correlation. (b) long period peaks of the CDF. (c) domain peaks in logarithmic scale. Indicated are the determination of the most probable layer thickness, l_t, and of the maximum layer extension, l_e. (d) Long period peaks in logarithmic scale. The shape of the CDF along the meridian (light line in (a) and (b)) is Ruland's interface distribution function (IDF).

Structure parameter extraction. Because of the broad layer thickness distributions the peaks of the amorphous layers are not separated from those of the crystalline lamellae. Only the most probable layer thickness, l_t, and the largest extension of lamellae, l_e, can be read directly from the CDF. In the logarithmic representation the determination of the triangle widths becomes more precise. In similar manner the long period peaks on the opposite side of the CDF can be evaluated, resulting in the most probable long period, L, and the lateral correlation of the long periods, L_e.

Non–isothermal crystallization

Similar structure in core and shell. Figure 8

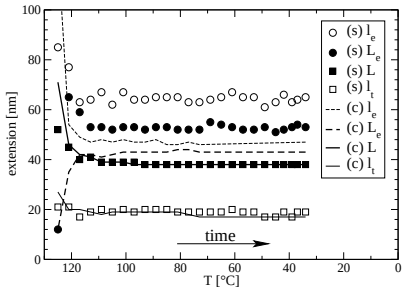

Figure 8: Non-isothermal, oriented crystallization after melting at 140°C of HPIM shell (s) and core (c) material. Nanostructure parameters as a function of decreasing temperature. l_e: lateral extension of the lamellae. L_e: lateral correlation among long periods. L: long period. l_t: most probable layer thickness.

demonstrates the evolution of the nanostructure parameters during non–isothermal crystallization as extracted from the CDFs. The four curves at the bottom of the drawing show that the evolution of domain thicknesses and domain arrangement along the shish is the same for core and shell material. On the other hand, the lateral structure (cf. the upper four curves) evolves differently in core and shell. In the core material lamellae with an extension l_e of 45 nm are observed. In the shell material the corresponding layer extension is 65 nm. In addition, the lateral range of correlations between surfaces of neighboring lamellae exhibit similar differences. Nevertheless, in the beginning of the crystallization we find that the first lamellae from the core (dashed curve) are much wider than the first lamellae of the shell material (open circles). We allocate this result to the already mentioned observation of incomplete melting of the HPIM lamellae in the case of the core material.

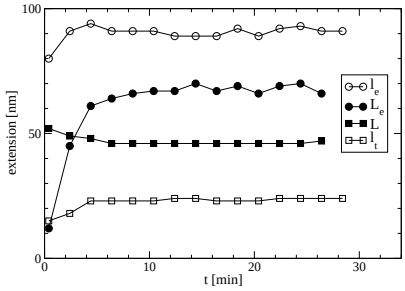

Figure 9: Isothermal (127 °C), oriented crystallization after melting at 140°C of HPIM shell material. Nanostructure parameters as a function of time after temperature jump. l_e: lateral extension of the lamellae. L_e: lateral correlation among long periods. L: long period. l_t: most probable layer thickness

Isothermal crystallization

Figure 9 demonstrates the evolution of nanostructure parameters as a function of time during the isothermal crystallization phase of the core material. Lamellae with an extension, l_e, of more than 90 nm are formed. The increase of the diameter is fast (4 min) for the individual layer. The increase of the lateral correlation between neighboring layers (L_e) takes more time. Not only the lateral layer extensions, but also layer thicknesses and long periods are higher than what has been found during non-isothermal crystallization. Nevertheless, the CDFs (Figure 10a) show a similar random arrangement of lamellae along the backbone as that observed during non-isothermal crystallization. After the isothermal period the material is quenched, and only during this part of the experiment a long ranging correlation is created, which is clearly emerging from the CDF.

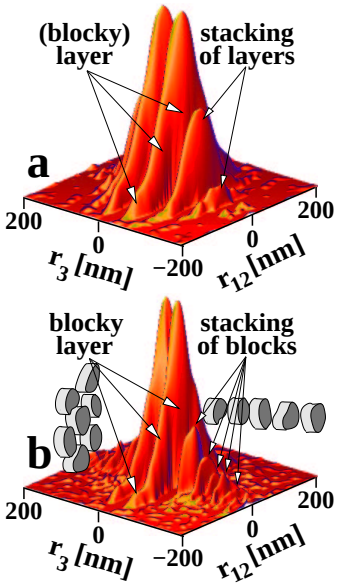

Figure 10: CDFs from the isothermal crystallization experiment. (a) at the end of the isothermal period. (b) at 59°C during quenching from the crystallization temperature. The domain peak face is shown in logarithmic scale

At the end of the isothermal period (Figure 10a) we observe thick and extended layers. In a logarithmic intensity scale the corresponding central triangular peaks in the CDF exhibit a faint modulation in lateral direction. Such modulation does not disagree with Strobl's model of building lamellae from blocks.[33–36] Two additional triangular peaks on each side of the equator indicate correlation between neighboring lamellae. Due to the fact that only two correlation peaks are visible (arrows), the inter-lamellar correlation is poor. Both the correlation peaks clearly show a triangular shape. Thus lamellae are correlated with each other as a whole, and a lateral offset is negligible. Nevertheless, many of the lamellae are not correlated ("solos").

During quenching (Figure 10b) the newly created crystallites form a completely different nanostructure. The central peaks still show the triangular "layer" shape. But now the layers are thinner, and, moreover, the peaks are clearly modulated in lateral direction exposing the block structure proposed by Strobl[33–36] and predicted from computer simulations of PE crystallization from an oriented amorphous state.[37] We observe that each lamella is made from one central block surrounded by a single or double ring of satellite blocks. The central part of the peak is related to the self-correlation of all blocks, the second maximum occurs when the ghost of the lamella is moved by one block diameter. The outmost maximum is generated from the correlation between opposite satellites. Roughly estimated, the distance between two adjacent blocks is 45 nm.

Along the principal axis (r_3) the correlation among crystallites has increased considerably. Five orders of correlation are clearly detectable. Thus there are clusters, in which up

to five crystalline domains are correlated ("quintets") in the direction of the shish. Nevertheless, the correlations do not concern lamellae any more. The lateral extension of the correlation peaks is not wider than the extension of a single block from the primary lamellae. We see a long period, because each block recognizes a long row of predecessors and successors (but not their satellites) along the fiber direction. We do not observe a layer line, because every individual block recognizes its satellites in lateral direction.

Outlook

We have studied the multidimensional aspects of nanostructure evolution in crystallization experiments of polyethylene and have demonstrated, that the resulting structure cannot be described by the notion of a perfect structure that has undergone some distortions. Our experiment shows that it is just the other way round: Random insertion of crystallites is preferred. Development of order is secondary. In polymer science there are many publications concerning structures derived by distortion of a perfect structure. On the other hand, stochastic structures, e.g. the random insertion of lamellae on a backbone, have rarely been studied. Thus in part 2[38] of this series we will explore the ideal stochastic process and its liquid scattering. By doing so we learn how to discriminate order from the natural correlations that come along with the dense random packing of domains. In statistical physics this process is named the "random car parking process".[39, 40]

Finally, in part 3,[41] we will return to the experimental data of our nanostructure evolution experiments. The last study is dedicated to the analysis of the 1D structure that is defined by the sequence of crystals along the shish. In the general chaos (explored in part 2) we look for order, i.e. clusters of several crystallites distinguished by a certain amount of order among them. Because of the structure evolution being documented in the time-resolved experimental data as a function of temperature, we then can start to describe the basic structure formation processes that are modifying the random nature of crystallization. The 1D data required for this study are found in the interface distribution function (IDF), that can be extracted from the CDF along the meridian (Figure 7a and b, light lines).

Acknowledgments. We acknowledge the Deutsche Elektronen Synchrotron (DESY) for provision of synchrotron radiation facilities at HASYLAB within the frame of the project II-01-041. One of us (A.A.C.) expresses his gratitude to the Deutscher Akademischer Austauschdienst (DAAD) for an awarded grant, which enables his studies at the University of Hamburg, Germany.

References

[1] G. Elsner, C. Riekel, H. G. Zachmann, in: H. H. Kausch, H. G. Zachmann, Eds. "Advances in Polymer Science", Springer, Berlin, vol. 67, **1984** pp. 1–58.
[2] S. F. Xavier, *Pop. Plast. Packag.* **1996**, *41*, 61.
[3] H. Ishida, P. Bussi, in: T.-W. Chou, Ed. "Mater. Sci. Technol.", VCH, Weinheim, Germany, vol. 13, **1993** pp. 339–79.
[4] S. Fakirov, N. Stribeck, A. A. Apostolov, Z. Denchev, B. Krasteva, M. Evstatiev, K. Friedrich, *J. Macromol. Sci. Phys.* **2001**, *40*, 935.
[5] K. Friedrich, E. Ueda, H. Kamo, M. Evstatiev, B. Krasteva, S. Fakirov, *J. Mater. Sci.* **2002**, *37*, 4299.
[6] R. H. Somani, B. S. Hsiao, A. Nogales, S. Srinivas, A. H. Tsou, I. Sics, F. J. Baltá Calleja, T. A. Ezquerra, *Macromolecules* **2000**, *33*, 9385.
[7] S. Yamazaki, M. Hikosaka, A. Toda, I. Wataoka, K. Yamada, K. Tagashira, *J. Macromol. Sci. Part B Phys.* **2003**, *B42*, 499.
[8] R. H. Somani, L. Yang, B. H. Hsiao, H. Fruitwala, *J. Macromol. Sci. Part B Phys.* **2003**, *B42*, 515.
[9] D. R. Rueda, F. Ania, F. J. Baltá Calleja, *Polymer* **1997**, *38*, 2027.
[10] N. Stribeck, R. Bayer, G. von Krosigk, R. Gehrke, *Polymer* **2002**, *43*, 3779.
[11] H.-G. Elias, *Polymere: Von Monomeren und Makromolekülen zu Werkstoffen*, Hüthig und Wepf, Zug, **1996**.
[12] P. Suaphol, J.-S. Lin, *Polymer* **2001**, *42*, 9617.
[13] K. Cho, D. N. Saheb, J. Choi, H. Yang, *Polymer* **2003**, *43*, 1407.
[14] C. De Rosa, O. Ruiz de Ballesteros, M. Di Gennaro, F. Auriemma, *Polymer* **2003**, *44*, 1861.
[15] C. G. Vonk, Y. Koga, *J. Polym. Sci. Polym. Phys.* **1985**, *23*, 2539.
[16] J. Wu, J. M. Schultz, J. M. Samon, A. B. Pangelinan, H. H. Chuah, *Polymer* **2001**, *42*, 7161.
[17] R. Bonart, *Kolloid Z. u. Z. Polymere* **1966**, *211*, 14.
[18] R. Bonart, R. Hosemann, *Kolloid Z. u. Z. Polymere* **1962**, *186*, 16.
[19] C. G. Vonk, G. Kortleve, *Kolloid-Z. u. Z. Polymere* **1967**, *220*, 19.
[20] G. R. Strobl, M. Schneider, *J. Polym. Sci., Part B: Polym. Phys.* **1980**, *B18*, 1343.
[21] N. Stribeck, *Anal. Bioanal. Chem.* **2003**, *376*, 608.
[22] N. Stribeck, *J. Appl. Cryst.* **2001**, *34*, 496.
[23] N. Stribeck, *Colloid Polym. Sci.* **2002**, *280*, 254.
[24] N. Stribeck, S. Fakirov, A. A. Apostolov, Z. Denchev, R. Gehrke, *Macromol. Chem. Phys.* **2003**, *204*, 1000.
[25] M. D. Buhmann, *Acta Numerica* **2000**, *9*, 1.
[26] N. Stribeck, S. Fakirov, *Macromolecules* **2001**, *34*, 7758.
[27] N. Stribeck, E. Buzdugan, P. Ghioca, S. Serban, R. Gehrke, *Macromol. Chem. Phys.* **2002**, *203*, 636.
[28] C. G. Vonk, *Colloid Polym. Sci.* **1979**, *257*, 1021.
[29] W. Ruland, *Colloid Polym. Sci.* **1977**, *255*, 417.
[30] W. Ruland, *Colloid Polym. Sci.* **1978**, *256*, 932.
[31] N. Stribeck, W. Ruland, *J. Appl. Cryst.* **1978**, *11*, 535.
[32] H. G. Kilian, W. Wenig, *J. Macromol. Sci. - Phys.* **1974**, *B9*, 463.

[33] B. Heck, T. Hugel, M. Iijima, E. Sadiku, G. Strobl, *New J. Phys.* **1999**, *1*, 17.1.
[34] T. Hugel, G. Strobl, R. Thomann, *Acta Polym.* **1999**, *50*, 214.
[35] B. Heck, T. Hugel, M. Iijima, G. Strobl, *Polymer* **2000**, *41*, 8839.
[36] M. Iijima, G. Strobl, *Macromolecules* **2000**, *33*, 5204.
[37] A. Koyama, T. Yamamoto, K. Fukao, Y. Miyamoto, *Phys. Rev. E* **2002**, *65*, 050801.
[38] N. Stribeck, *Macromol. Chem. Phys.* **2004**, *submitted*.
[39] J. W. Evans, *Rev. Mod. Phys.* **1993**, *65*, 1281.
[40] B. Bonnier, D. Boyer, P. Viot, *J. Phys. A* **1994**, *27*, 3671.
[41] N. Stribeck, A. Almendarez Camarillo, R. Bayer, *Macromol. Chem. Phys.* **2004**, *submitted*.

Synopsis. Highly oriented crystallization of PE lamellae is observed in a time-resolved experiment. The data show that the crystalline domains are more or less placed at random. The oriented SAXS data permit to discuss layer dimensions and perfection as a function of different processing during crystallization.